

# Coordination-Dependent Kinetics in the Catalysis of Gold Nanoclusters

Forrest H. Kaatz,\* Dmitry Yu. Murzin, and Adhemar Bultheel

Cite This: *ACS Catal.* 2021, 11, 9073–9085

Read Online

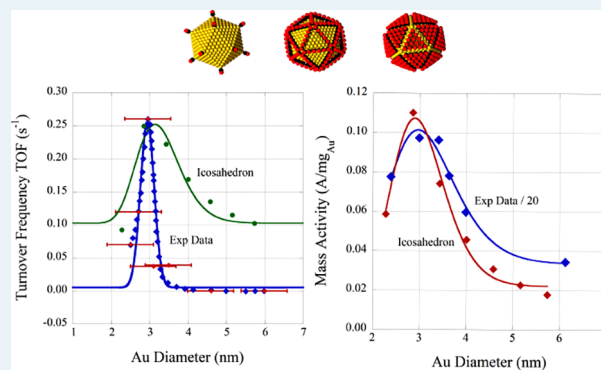
ACCESS |

Metrics &amp; More

Article Recommendations

**ABSTRACT:** A coordination-based kinetic model was used to explore the turnover frequency (TOF) in the oxidation of carbon monoxide on gold polyhedral nanoclusters. The Debye energy model was used to determine the Gibbs energy of bare nanoclusters. An empirical energy model derived from density functional theory (DFT) and thermodynamics was used to determine the size dependence of the Gibbs adsorption energy. A thermodynamic approach was used to model the kinetics of CO oxidation on gold nanoclusters. The adsorption was modeled with a Langmuir–Hinshelwood (L-H) mechanism and also a mechanism (Eley–Rideal, E-R) where oxygen interacts with sites on the cluster support. The coordination, shape, and the Gibbs energy of adsorption were found to be important factors in replicating experimental TOF dependencies. The data from the L-H mechanism was shown to model the experimental results more closely. The mass activity of icosahedra for this reaction shows a good similarity with the experimental data. This work provides guidance for different distributions due to shape and size when determining the TOF and the mass activity.

**KEYWORDS:** catalysis, reaction kinetics, coordination, nanoclusters, mass activity, Au



## INTRODUCTION

It was suggested long ago by Boudart that catalytic reactions depend on structure and shape and thus the coordination of the catalyst.<sup>1</sup> Later, Falicov and Somorjai proposed that coordination-sensitive edge and kink sites would be most likely responsible for structure-sensitive reactions.<sup>2</sup> Nanocluster synthesis has reached the stage where narrow particle size distributions of the desired shapes of many elements and alloys may be achieved.<sup>3</sup> This allows experimentalists to fine-tune catalytic reactions so that specific shapes, sizes, and thus the coordination of the catalyst is known. The current work focuses on modeling the kinetics, or turnover frequency (TOF) and mass activity, of surface sites, showing that they strongly depend on the shape and structure of nanoclusters. More specifically, we study the oxidation of carbon monoxide on gold nanoclusters with specific sizes and shapes. The size range we investigate (2–6 nm) has produced polyhedra in a limited number of cases,<sup>4</sup> and we argue that model structures are useful for showing trends and data in this size range. Further work may elucidate the contribution of defects and nonuniform structures.

Gold catalysis started to be widely studied about 30 years ago.<sup>5</sup> Although bulk gold is normally inert, Haruta et al. showed in 1987 that nanogold is an effective catalyst,<sup>6–8</sup> with a potential to be used in chemical, biomedical, and plasmonic applications.<sup>9</sup> In particular, Haruta's group measured the TOF for the

oxidation of carbon monoxide on gold nanoparticles.<sup>10,11</sup> Coordination- and size-dependent CO oxidation was explored in this work using a kinetic modeling approach.

Recently, coordination-specific magic formulas for the surface sites of 19 different nanoclusters were determined.<sup>12,13</sup> These magic formulas can assist the understanding of the coordination- and size-dependent surface behavior of nanoclusters. In the size dimension of the mesoscale, neither atomic nor bulk concepts apply, and activity reflects the surface coordination of the specific cluster being studied. While the exact dimensions of the mesoscale are ambiguous, a good approximation is nanoclusters with diameter  $D \sim 5–100$  nm. Density functional theory, (DFT) studies on the surface states of nanoclusters show that when  $D \sim 3$  nm for gold,<sup>14</sup> and about  $D \sim 2$  nm, for platinum,<sup>15</sup> the transition of surface states from the atomic to bulk has occurred. In addition, Hoover et al. calculated that the difference in entropy between the thermodynamic prediction and the exact entropy is less than  $k_B$  (Boltzmann's constant) when the number

Received: February 24, 2021

Revised: June 14, 2021

of atoms,  $N > 400$ , for close packed cubes.<sup>16</sup> Similarly, an estimate of  $D$  as a lower limit of the mesoscale can be made from thermal fluctuations.<sup>17</sup> For a cube of diameter  $D$  and side  $S$ , with  $\rho$  atoms per unit volume, the thermal fluctuations are about  $\delta T/T \approx (\rho S^3)^{-1/2}$ . For solids and liquids,  $\rho \approx 50/\text{nm}^3$ . Assuming fluctuations of  $10^{-2}$ , this gives  $S \approx 5$  nm. The size dimension in this study is in the range  $D \sim 2\text{--}6$  nm. This size regime is of current interest and active research.<sup>18</sup>

The thermodynamics of nanoscale systems was studied many years ago by Hill.<sup>19</sup> However, the scaling of Hill's nanothermodynamics and the formulation by Gibbs has recently been shown to be equivalent,<sup>20</sup> for surfaces of constant curvature, or spheres. We study polyhedra, where the thermodynamic properties deviate from spherical by the scaling of the anisotropy of the polyhedra.<sup>21</sup> Thus, our modeling based on Gibbs thermodynamics is assumed to be accurate with scaling of the anisotropy of the different polyhedra.

The potential nonmetallic character of gold clusters was discussed by Bond,<sup>22</sup> who collected the available literature confirming that below a certain size gold clusters exhibit nonmetallic and nonconductive features. The critical size for the transition between the nonmetallic and metallic behavior depends among other parameters such as the support interaction and formation processes. It seems that there is no general agreement at which size high catalytic activity is associated with the nonmetallic character with the corresponding values ranging between 1.5 and 2.5 nm. An apparent difficulty in assessing the transition between the metal to nonmetal is inaccessibility of reliable DFT calculations for clusters of such size. In any case, very small gold nanoparticles (1–2 nm) should be essentially nonmetallic, still exhibiting low reactivity. The reactivity of gold nanoparticles should be thus discussed in terms of CO and oxygen binding for nanosized clusters as done in the current work, as this is central to understanding the enhanced catalytic properties for supported Au nanoparticles compared to bulk Au (for example, see ref 14, as already mentioned).

Different kinetic models for CO oxidation over gold were evaluated in ref 23, considering both molecular or dissociative oxygen adsorption. In the latter case, the specific role of the support should be emphasized as homolytic dissociation of oxygen requires two sites, one on the surface of a gold cluster and another one on the support. The kinetic model for the dissociative adsorption also included the so-called jumps of atomically adsorbed oxygen between the sites. An alternative conventional mechanism also discussed in ref 23 relies on the concept of an unlimited adsorbed overlayer. A detailed analysis presented in ref 23 confirmed that the conventional approach can be safely applied for the cases when the reaction itself is not rapid, which often is the situation observed experimentally. Subsequently, in the current work, the Langmuir–Hinshelwood type of models developed for extended surfaces was applied, neglecting the lateral interactions between the adsorbed species. According to ref 23, such interactions, even if present, do not seem to be critical for interpretation of the experimental data on CO oxidation.

Adsorption energy depends linearly on what is defined as the generalized coordination,<sup>24,25</sup> which for some compounds is the generalized coordination of the adsorption site. For the adsorption of CO on gold, a few studies have been done.<sup>26,27</sup> In particular, Xu et al.<sup>27</sup> studied neutral, anion, and cation gold clusters with DFT calculations of the adsorption energy of CO and O<sub>2</sub>. Gold anion clusters are thought to mimic charge

redistribution from an oxide substrate.<sup>27–29</sup> Furthermore, the Gibbs adsorption energy has been calculated by several authors using a DFT approach.<sup>30,31</sup> We find it convenient to model the Gibbs adsorption energy with a thermodynamic approach, which is computationally robust. For the bare clusters, we calculate the Gibbs energy using the Debye model, which has been applied to structural transitions in Ag–Au nanoparticles.<sup>32</sup> A coordination approach using empirical energy methods, derived from DFT, along with thermodynamics to complete the Gibbs adsorption energy calculation is provided herein.<sup>33,34</sup> This enables the determination of  $\Delta G$  as a function of size and coordination, with a unique approach different from that reported in the literature so far.

At this point, some comments can be made regarding analysis of DFT-related catalytic calculations. Adsorption of reacting molecules depends on DFT functionals, and as recently shown by refs 35 and 36, systematic errors can occur in the DFT calculations. It is not completely clear how these errors affect the adsorption energies of CO and O<sub>2</sub> on gold nanoclusters as the specifics of adsorption with nanocluster coordination has not been determined. Some data<sup>37</sup> indicates the coordination of the adsorption site is relevant for CO catalysis. The data used herein<sup>27</sup> may need to be revised in the future, but at the present time, they are the most accurate. With regard to the TOF on nanoclusters, some work has been done using DFT and kinetic Monte Carlo studies of the TOF on platinum nanoclusters.<sup>38</sup> This may provide an alternate approach to study the oxidation of CO on gold. For gold nanoclusters, some previous work indicates that corner and kink sites are important in this reaction.<sup>39,40</sup> Our goal is to elucidate the importance of coordination, size, and shape on the TOF and mass activity for the oxidation of carbon monoxide on gold nanoclusters.

## METHODS

The novel methods proposed in this work are divided into sections to clarify the procedures. The Gibbs energy calculation will be discussed first. In the discussion that follows, we use the terms “cluster” or “nanocluster” to refer to polyhedra of 1–10 nm, “subnanocluster” to refer to clusters <1 nm, and “nanoparticle” to refer to a collection of atoms with any defined geometry.

**Gibbs Energy.**  $G$  is defined below as the size-dependent Gibbs energy of the cluster. Because of adatoms, like CO or O<sub>2</sub>, being bonded to the outer shell atoms there is an increase in  $G$  that is called the adsorption energy and is denoted as  $\Delta G$ . This can be split up over different coordination types of the atoms on the outer shell bonding to adatoms. For example, a kink atom adds to the adsorption energy with an amount  $\Delta G_k$ . Similarly, an edge atom adds  $\Delta G_e$ , while a facet atom contributes  $\Delta G_f$  then<sup>41</sup>

$$\Delta G = \sum_{o \in \{f, e, k\}} \Delta G_o N_o \quad (1)$$

where  $N_o$  is the number of atoms in the outer shell of the indicated type. The total number of atoms in the outer shell bonded to adatoms is defined as  $N_s = N_f + N_e + N_k$ , resulting in

$$\Delta G = \Delta G_f \cdot (1 - f_e - f_k) + \Delta G_e \cdot f_e + \Delta G_k \cdot f_k \quad \text{where} \\ f_o = N_o/N_s, o \in \{e, k\} \quad (2)$$

with the Gibbs energy fraction expressed through the edge and kink sites which have explicit coordinations for specific structures—as detailed in Table 1. In Table 1,  $n$  refers to

**Table 1. Formulas for Nanocluster Shapes**<sup>12,13,a</sup>

<i>cn</i>	fcc truncated cube	<i>cn</i>	icosahedron	<i>cn</i>	octahedron
5	12 <i>n</i> - 12	6	12	4	6
7	24	8	30 <i>n</i> - 30	7	12 <i>n</i> - 12
8	12 <i>n</i> <sup>2</sup> - 12 <i>n</i> - 18	9	10 <i>n</i> <sup>2</sup> - 30 <i>n</i> + 20	9	4 <i>n</i> <sup>2</sup> - 12 <i>n</i> + 8
<i>N</i> <sub>S</sub>	12 <i>n</i> <sup>2</sup> - 6	<i>N</i> <sub>S</sub>	10 <i>n</i> <sup>2</sup> + 2	<i>N</i> <sub>S</sub>	4 <i>n</i> <sup>2</sup> + 2
<i>N</i> <sub>T</sub>	4 <i>n</i> <sup>3</sup> + 3 <i>n</i> <sup>2</sup> + 3 <i>n</i> - 7	<i>N</i> <sub>T</sub>	$\frac{10}{3}n^3 - 5n^2 + \frac{11}{3}n - 1$	<i>N</i> <sub>T</sub>	$\frac{2}{3}n^3 + 2n^2 + \frac{7}{3}n + 1$
<i>cn</i>	decahedron	<i>cn</i>	fcc cuboctahedron		
4	5	5	12		
6, 8	5 <i>n</i> - 3, 10 <i>n</i> - 10	7	24 <i>n</i> - 24		
9	5 <i>n</i> <sup>2</sup> - 15 <i>n</i> + 10	8, 9	6 <i>n</i> <sup>2</sup> - 12 <i>n</i> + 6, 4 <i>n</i> <sup>2</sup> - 12 <i>n</i> + 8		
<i>N</i> <sub>S</sub>	5 <i>n</i> <sup>2</sup> + 2	<i>N</i> <sub>S</sub>	10 <i>n</i> <sup>2</sup> + 2		
<i>N</i> <sub>T</sub>	$\frac{5}{6}n^3 + \frac{5}{2}n^2 + \frac{8}{3}n + 1$	<i>N</i> <sub>T</sub>	$\frac{10}{3}n^3 - 5n^2 + \frac{11}{3}n - 1$		

<sup>a</sup>The variable *cn* refers to the ordinary coordination number and *n* the number of shells in the cluster.

complete shells of atoms in the clusters. Note that eq 2 applies to adsorption to on-top sites; otherwise, not all atoms will be bonded to atoms in the outer shell. Also, eq 2 refers to clusters with complete shells (no vacancies or defects) and treats all facet atoms as having similar reactivity, which is probably simplifying reality. Recently, increased control of kink, edge, and facet synthesis of nanocrystals has been demonstrated, although controlled size growth of polyhedra for 2 nm < *D* < 10 nm remains challenging.<sup>42</sup>

Two fundamental relationships on a per-particle basis will be applied. For the Gibbs energy and adsorption constant, *K<sub>a</sub>*, it holds:

$$K_a = \exp\left(-\frac{\Delta G}{RT}\right) \quad (3)$$

where *R* is the gas constant and *T* is the temperature in Kelvin. In addition, Brønsted–Evans–Polanyi relationships are widely used in homogeneous and heterogeneous catalysis<sup>41,43</sup> using a relationship for reaction constants *k* and equilibrium constants *K* as follows:

$$k = gK^\alpha, \quad 0 < \alpha < 1 \quad (4)$$

where *g* and  $\alpha$  (Polanyi parameter) are constants. The Polanyi parameter is unitless and a proper fraction, as given originally by Brønsted.<sup>44</sup> In the current work, the BEP relationship was used linking kinetics with thermodynamics through eq 4. Equation 4 reflects the original proposal of Brønsted who was considering decomposition of nitroamide. Extension of this approach by Evans and Polanyi as well as Horiuti to activation energy analysis allowed utilization of the linear free energy relationship (LFER) to calculate the activation energy of many reactions, catalytic ones or proceeding without any catalyst through the following relationship

$$\Delta E \sim \alpha \Delta Q \quad (5)$$

where  $\alpha$  is the Polanyi parameter. The BEP approach was successfully used to examine many reactions on metal surfaces including hydrogenation and dehydrogenation of ethylene,<sup>45</sup> ammonia synthesis,<sup>46</sup> and even reactions on metal oxides, as for example different oxidation reactions,<sup>47</sup> including oxidation of CO.<sup>48</sup>

In a general case, the slope of eq 5 and thus the value of Polanyi parameter can be different depending on the crystallographic face,<sup>49</sup> as demonstrated for the activation energy of CH,

CO, and trans COOH dissociation reactions on (100), (110), and (111) surfaces of several metals. In the latter case, the BEP relation was valid when the overall transition state (TS) is not varying at the conditions for which LFER is applied.

The oxidation of CO on gold clusters and the applicability of LFER was recently assessed.<sup>50</sup> It was concluded that all the reaction barriers relevant for CO oxidation exhibit linear scaling relationships with CO and oxygen binding strength. The authors explored planar clusters of different size concluding that only extremely small subnanoclusters with just 3 to 5 gold atoms are different from larger ones because of their significantly different local surface atoms arrangement. Liu et al.<sup>50</sup> showed that the Polanyi parameter was approximately the same for different gold nanoclusters, and ca. 0.5 in magnitude. In the current work, it was considered that clusters of different shape display the same Polanyi parameter, based on similar transition states; thus, a single value of the Polanyi parameter equal to 0.5 was taken in our calculations. Recent studies by Behraves et al.<sup>51</sup> argued against the dissociative adsorption of oxygen and conclude that for the oxidation of CO there is a linear relationship between the activation energy and the energy of adsorption.

We then have

$$k = k'_a \exp(-\alpha(f_{n,e} \cdot \chi_e(D) + f_{n,k} \cdot \chi_k(D))) \quad (6)$$

where

$$\chi_e(D) = \frac{\Delta G_e(D) - \Delta G_f(D)}{RT},$$

$$\chi_k(D) = \frac{\Delta G_k(D) - \Delta G_f(D)}{RT} \quad (7)$$

and

$$k'_a = g \exp\left(-\alpha \frac{\Delta G_f}{RT}\right) \quad (8)$$

The  $\chi_{e,k}$  calculations are important for the determination of the TOF, as is shown below. The explanation of the method to calculate  $\Delta G$  is provided below.

**Debye Energy Model.** The Gibbs free energy of the bare catalyst can be described through the Debye model, which has successfully modeled the size dependence of the Gibbs energy,<sup>32,52–54</sup>

$$G_{clean} = F + PV_m \quad (9)$$

where  $F$  is the free energy and  $PV_m$  is the nonzero pressure volume term, with  $V_m$  the molar volume. If one studies the original Debye model,<sup>52</sup> a Morse potential is used and gold is not considered, as this is hardly an appropriate potential for gold. Nevertheless, the Debye model was successfully used for structural transitions in Ag–Au alloy nanoparticles<sup>32</sup> and was used here for gold clusters. In the Debye model, the free energy is

$$F(T, V) = E_{coh}(V) + E_D(V, T) - TS_D(V, T) \quad (10)$$

where  $E_{coh}$  is the cohesive energy. The Debye model gives the vibrational lattice energy  $E_D$  and the entropy  $S_D$  as

$$E_D(T, V) = 3k_B TB(\Theta/T) + 9k_B \Theta_0/8 \quad (11)$$

where  $B(\Theta/T)$  is the Debye function, in terms of the Debye temperature  $\Theta$ . For gold,  $\Theta_0 = 176K$ .<sup>55</sup>

$$B(\Theta/T) = 3(T/\Theta_0)^3 \int_0^{\Theta_0/T} \left( \frac{x^3}{e^x - 1} \right) dx \quad (12)$$

and  $S_D$  is

$$S_D(V, T) = 4k_B \left[ B(\Theta/T) - \frac{3}{4} \ln(1 - e^{-(\Theta_0/T)}) \right] \quad (13)$$

For a nanocluster, the following changes are noted where  $x_s$  and  $\omega_s$  are the surface vibrational amplitude and frequency<sup>56</sup>

$$\frac{x_s}{x_b} = 1.43 \quad \text{and} \quad \frac{\omega_s}{\omega_b} = 0.404 \quad (14)$$

where the subscript  $b$  refers to the bulk. These results are qualitatively in agreement with more recent data,<sup>57</sup> showing a linear relationship with the diameter of the nanoclusters, or proportional to the bulk as shown here.

Then the vibrational lattice energy of a surface atom is

$$E_D^s(V, T) = \left( \frac{x_s}{x_b} \right)^2 E_D(V, T) = 6.135k_B TB(\Theta/T) \quad (15)$$

In statistical mechanics terms, when the vibrational frequency changes one gets<sup>54</sup>

$$\Delta S_D = 3k_B \ln(\omega_b/\omega_s) \quad (16)$$

and the vibrational entropy change of a surface atom is

$$\begin{aligned} S_D^s(V, T) &= S_D(V, T) + \Delta S_D \\ &= 4k_B \left[ B\left(\frac{\Theta}{T}\right) - \frac{3}{4} \ln(1 - e^{-(\Theta_0/T)}) \right] + 2.719k_B \end{aligned} \quad (17)$$

Then the free energy of the bulk and surface terms is

$$\begin{aligned} F(V, T) &= N_T E(V) + (N_T - N_s)[E_D(V, T) \\ &\quad - TS_D(V, T)] + N_s[E_D^s(V, T) - TS_D^s(V, T)] \end{aligned} \quad (18)$$

or

$$\begin{aligned} F(V, T) &= E_{coh} + \frac{3RT}{10^3} \ln \left( 1 - \exp \left( -\frac{\Theta_0}{T} \right) \right) - \frac{RT}{10^3} B\left(\frac{\Theta}{T}\right) \\ &\quad + \frac{4\alpha_s d_{Au} RT}{10^3 D} \left( 3B\left(\frac{\Theta}{T}\right) - 2.719 \right) \end{aligned} \quad (19)$$

where the units of  $F(V, T)$  are kJ/mol. The size and shape dependence of the cohesive energy is

$$E_{coh} = E_b \left( 1 - \frac{3\alpha_s d_{Au}}{D} \right) \quad (20)$$

here  $E_b = -367.6$  kJ/mol for Au and  $d_{Au} = 0.292$  nm. The shape factor  $\alpha_s$  is defined as  $S'/S$ , where this ratio represents the surface area of the polyhedron relative to a sphere.<sup>58</sup> The pressure volume term in terms of the Laplace–Young equation is<sup>59</sup>

$$P = \frac{4f}{D} \quad (21)$$

where  $f = 2.097$  J/m<sup>2</sup> and for gold  $V_m = 10.2$  cm<sup>3</sup>/mol. Table 2 tabulates the relevant surface area and shape factors for the polyhedra considered in this manuscript.

**Table 2. Values for  $A_s$ , the Surface Area of the Polyhedra, and  $\alpha_s$ , the Shape Factor<sup>a</sup>**

shape	$A_s$	shape factor $\alpha_s$
icosahedron	$(5\sqrt{3})(n \cdot r(cn))^2$	1.065
cuboctahedron	$(6 + 2\sqrt{3})(n \cdot r(cn))^2$	1.105
octahedron	$(2\sqrt{3})(n \cdot r(cn))^2$	1.183
truncated cube	$12(n \cdot r(cn))^2$	1.24
decahedron	$\frac{5\sqrt{3}}{2}(n \cdot r(cn))^2$	1.254

<sup>a</sup>The term  $n$  is the number of shells, and the term  $r(cn)$  is defined below in eq 32.

Then for  $PV_m$  one gets for gold

$$PV_m = \frac{4f}{D} V_m = \frac{21.34}{D} \text{kJ/mol} \quad (22)$$

with  $D$  in nm. Here  $D$  is the effective diameter, or largest distance across the nanocluster, which we use computationally, and can also be determined experimentally. Figure 1 shows the Gibbs energy as a function of temperature and diameter, with special emphasis on the size range considered here.

**Gibbs Energy of Adsorption.** The change in free energy upon adsorption is<sup>34</sup>

$$\begin{aligned} \Delta G_{ad}(T, P) &= G(T, p, N_{ad}) - G(T, p, 0) \\ &= \frac{N_{ad} R d_{Au}^2}{10^3 k_B A_s} (E_{ad} - \Delta\mu_{ad}(T, p)) \end{aligned} \quad (23)$$

where  $E_{ad}$  is the energy of adsorption of adsorbates (in eV) calculated by DFT,  $d_{Au} = 0.292$  nm (gold atom diameter) and  $R/(10^3 k_B)$  is a conversion factor to give kJ/mol. In reference 34, the factor  $Rd_{Au}^2/(10^3 k_B A_s)$  in the Gibbs adsorption energy, eq 23, was left out. This may be relevant for DFT calculations but cannot be correct for clusters as the term  $N_{ad}$  (number of adsorbates) rapidly causes the Gibbs energy to become larger than the entire cluster (see Figure 1). Thus, the scaling factor to modify the adsorption energy is used. This factor causes the facet Gibbs energy to become horizontally constant with large cluster size and the edge and kink Gibbs energy to approach zero for large clusters. This follows logically from the mathematics of the magic formulas for kinks, edges, and facets. When this factor is included, the surface Gibbs adsorption energy is an appropriate fraction of the total cluster Gibbs energy. Note that in eq 23, the

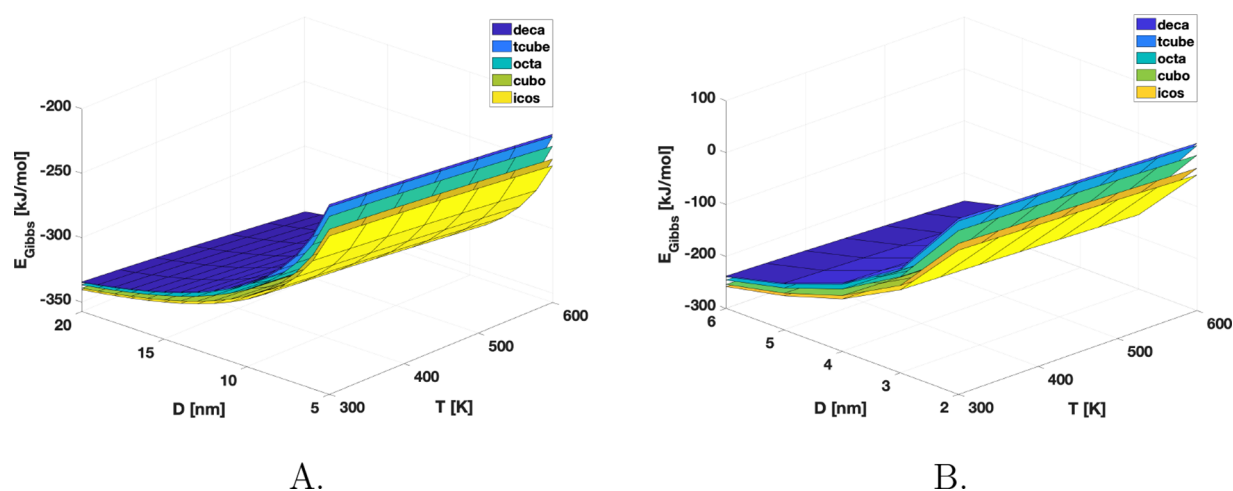


**Figure 1.** A. Gibbs energy for the five gold shapes under consideration. B. Size range of interest in this manuscript.

term  $G_{clean}(T, p, 0)$  is determined by the analysis in the preceding section. We emphasize that  $G_{clean}$  was determined in the previous section to provide a relevant scale of magnitude of the Gibbs adsorption energy versus that of the clean nanocluster.

The chemical potential  $\mu$  is defined as follows:<sup>33</sup>

$$\mu = \left( \frac{\partial G}{\partial N} \right)_{T,p,N} = \frac{G}{N} \quad (24)$$

using Maxwell's thermodynamic relations

$$dG = \left( \frac{\partial G}{\partial T} \right)_p dT + \left( \frac{\partial G}{\partial p} \right)_T dp = -SdT + Vdp \quad (25)$$

Considering the ideal gas law  $pV = Nk_B T$  one gets

$$\left( \frac{\partial G}{\partial p} \right)_T = V = \frac{Nk_B T}{p} \quad (26)$$

In turn, a finite pressure change from  $p$  to  $p^0$  results in

$$G(T, p) - G(T, p^0) = Nk_B T \ln(p/p^0) \quad (27)$$

Combining the above equations gives

$$\Delta\mu_{ad}(T, p) = \mu_{ad}(T, p^0) + 1/2k_B T \ln(p/p^0) \quad (28)$$

The zero reference state was chosen to be the total energy in an isolated molecule i.e.  $\mu_{ad}(T, p^0) = 1/2E_i$  where  $i$  refers to the isolated molecule. Then using  $E = G = H - TS$ , we have

$$\mu_{ad}(T, p^0) = 1/2[H_{ad}(T, p^0) - H_{ad}(0, p^0)] - 1/2T[S_{ad}(T, p^0) - S_{ad}(0, p^0)] \quad (29)$$

where  $H$  and  $S$  are obtained from thermochemical tables at  $p^0 = 1$  atm.<sup>60</sup> For  $O_2$  one obtains  $\mu_{O_2}(T, p^0) = -0.274$  eV, while for CO, it is  $-0.262$  eV at 300 K. From the experimental data,<sup>11</sup> we have that the total pressure is 40 Torr, with a 1:5 molar ratio of  $CO:O_2$ . Thus, we have that the partial pressures are  $p_{CO} = 8$  Torr and  $p_{O_2} = 32$  Torr. Using this data, one gets that  $\Delta\mu_{CO} = -0.321$  eV and that  $\Delta\mu_{O_2} = -0.315$  eV, from eq 28.

To allow for small deviations from the average bond length,  $i$  and  $j$  are defined as nearest neighbors, which are separated from the rest by requiring that  $r_{ij} < r_c$  where  $r_c$  is a threshold value, appropriate for the nanocluster. The value for  $r_c$  must be less

than the distance for second nearest neighbors and varies with the crystal structure.<sup>13</sup> For fcc crystals,  $r_c < 1.41 \cdot r_{min}$ , where  $r_{min}$  is the smallest bond length.<sup>13</sup> The value 1.41 is the scaled distance factor for second nearest neighbors, when the nearest neighbors are scaled to unit distance. Thus,

$$\mathbf{A}(i, j) = \begin{cases} 1, & \text{if } r_{ij} < r_c \text{ and } i \neq j \\ 0, & \text{otherwise} \end{cases} \quad (30)$$

describes the adjacency matrix for the cluster, and

$$\mathbf{E}(i, j) = \begin{cases} r_{ij}, & \text{if } r_{ij} < r_c \text{ and } i \neq j \\ 0, & \text{otherwise} \end{cases} \quad (31)$$

describes the Euclidean matrix for the cluster. An adjacency matrix and Euclidean matrix are used to determine the diameter,  $D$ , of the nanoclusters,<sup>12</sup> where the bond length in the clusters depends on the average coordination, see reference 56:

$$r(cn) = \frac{2r_B}{\left( 1 + \exp\left( \frac{12 - \langle cn \rangle_c}{8 \cdot \langle cn \rangle_c} \right) \right)} \quad (32)$$

Here  $r_B$  is the bulk bond length (0.2884 nm) and  $\langle cn \rangle_c$  is the average coordination of the cluster. A linear relationship exists between  $D$  and  $n$ , the number of cluster shells, as is shown in Table 3:

$$D(n) = a \cdot r_B \cdot n + b \quad (33)$$

These relationships produce diameters in agreement with other data. For the cuboctahedra with  $N$  equal to 55, 561, and 923, one gets diameters of 1.12, 2.85, and 3.43 nm, fairly close to published results for 55 atoms of 1.1 nm;<sup>61</sup> for 561 atoms, 2.7 nm;<sup>14</sup> and for 923 atoms, 3.5 nm.<sup>61</sup>

**Table 3.** Linear Constants for  $D(n)$

$a$	$b$	nanocluster
2.404	-0.3632	Au truncated cube
2.000	-0.0382	Au cuboctahedron
2.000	-0.0292	Au icosahedron
1.648	-0.0462	Au decahedron
1.415	-0.0428	Au octahedron

The energies of adsorbates have been shown to scale linearly with generalized coordination.<sup>24,25</sup> According to a DFT model for energies of adsorbates:<sup>24</sup>

$$\overline{CN}_i = \sum \frac{cn_j \cdot n_j}{cn_{\max}} \quad (34)$$

where the sum is over all nearest neighbors of  $i$ ,  $cn_{\max} = 12$  for top sites, 18 for bridge sites and has other values for other types of sites.<sup>24</sup> In this equation  $n_j$  is the number of nearest neighbors, and  $cn_j$  the coordination number of site  $j$ ; hence, each neighbor  $j$  of atom  $i$  has a weight of  $n_j/cn_{\max}$  associated with the site. The current approach gives data for octahedra which agrees well with the data of ref 62 (see their Figure 1). Adsorbate energy is linear with generalized coordination:<sup>24</sup>

$$E_{ad} = \overline{CN}_0 + m \cdot \overline{CN}_i \quad (35)$$

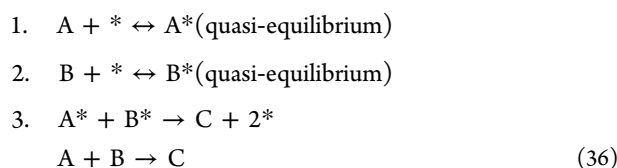
Here  $\overline{CN}_0$  is the linear intercept and  $\overline{CN}_i$  is defined as in eq 34. Table 4 below shows the values of the linear fits as determined by eq 35. These are determined from DFT calculations from reference 27.

**Table 4. Linear Fit of  $E_{ad}$  for Adsorption for Neutral and Anionic Gold Clusters<sup>a</sup>**

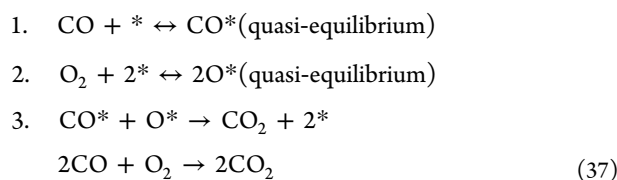
species	$\overline{CN}_0$ (eV)	slope $m$	charge
Au-CO	-1.44	0.15	neutral
Au-CO	-1.38	0.14	anion
Au-O <sub>2</sub>	-0.94	0.16	neutral
Au-O <sub>2</sub>	-0.93	0.15	anion

<sup>a</sup>Determined from DFT calculations from reference 27.

**Langmuir–Hinshelwood Mechanism.** In general, the TOF for reactions may display structure sensitivity which increases or decreases with size, or passes through a maximum.<sup>63</sup> Alternatively, there are structure-insensitive reactions with size-independent TOF. The Au-CO TOF has been experimentally observed to pass through a maximum for  $D \sim 2-5$  nm.<sup>10,11</sup> The literature discusses several types of reactions, including a two-step sequence and its corollary, the Eley–Rideal reaction, and the Langmuir–Hinshelwood (L-H) mechanism.<sup>64</sup> The L-H mechanism is relevant for surface reactions<sup>65</sup> and can be presented for molecular adsorption of both reactants:



where A and B are reactants, C is the product, and \* is a vacant surface site. The Au-CO oxidation follows a L-H mechanism<sup>66,67</sup> with dissociative adsorption of oxygen, as shown below:



so that in the general scheme of eq 36 above A is CO and B is O<sub>2</sub>. From the quasi-equilibria:

$$K_1 = \frac{\theta_{CO}}{P_{CO} \cdot \theta_v} \quad \text{or} \quad \theta_{CO} = K_1 P_{CO} \theta_v \quad (38)$$

$$K_2 = \frac{\theta_O^2}{P_{O_2} \cdot \theta_v^2} \quad \text{or} \quad \theta_O = \sqrt{K_2 P_{O_2}} \theta_v \quad (39)$$

where  $\theta_{CO}$ ,  $\theta_O$ , and  $\theta_v$  are respectively the coverage of CO, O, and the fraction of vacant sites. The balance equation is

$$\sum \theta_i = 1 \quad \text{or} \quad \theta_{CO} + \theta_O + \theta_v = 1 \quad \text{or} \quad \theta_v (K_1 P_{CO} + \sqrt{K_2 P_{O_2}} + 1) = 1 \quad (40)$$

The reaction rate for the general form of the L-H mechanism is<sup>64</sup>

$$v(D) = k_3 \theta_{CO} \theta_O = \frac{k_3 K_1 P_A K_2 P_B}{(1 + K_1 P_A + K_2 P_B)^2} \quad (41)$$

while for the specific case of CO oxidation, the TOF is

$$v(D) = \frac{k_3 K_1 P_{CO} \sqrt{K_2 P_{O_2}}}{(1 + K_1 P_{CO} + \sqrt{K_2 P_{O_2}})^2} \quad (42)$$

where

$$K_1(D) = K_A \exp\{-(f_e \cdot \chi_e^A(D) + f_k \cdot \chi_k^A(D))\} \\ = K_A \exp\{-(\xi_{e,k}^A(D))\} \quad (43)$$

$$K_2(D) = K_B \exp\{-(f_e \cdot \chi_e^B(D) + f_k \cdot \chi_k^B(D))\} \\ = K_B \exp\{-(\xi_{e,k}^B(D))\} \quad (44)$$

where  $k_3$  is the reaction rate constant for step 3,  $P_A$  and  $P_B$  are partial pressures or concentrations (for liquids) of A and B. For reaction 3, one gets

$$k_3(D) = K_C \exp\{(1 - \alpha)[f_e \cdot (\chi_e^A(D) + \chi_e^B(D)) \\ + f_k \cdot (\chi_k^A(D) + \chi_k^B(D))]\} \quad (45)$$

After some simplification<sup>64</sup>

$$v(D) = \frac{p_1 \exp\{(-\alpha)[f_{n,e} \cdot (\chi_e^A(D) + \chi_e^B(D)) + f_{n,k} \cdot (\chi_k^A(D) + \chi_k^B(D))]\}}{[1 + p_2 \exp\{-[\xi_{e,k}^A(D)]\} + p_3 \exp\{-[\xi_{e,k}^B(D)]\}]^2} \quad (46)$$

where

$$p_1 = k_3 K_{CO} P_{CO} \sqrt{K_{O_2} P_{O_2}} = k_3 p_2 p_3 \quad \text{and} \quad p_2 = K_{CO} P_{CO} \quad \text{and} \\ p_3 = \sqrt{K_{O_2} P_{O_2}} \quad (47)$$

where  $p_1$  is a lumped frequency constant and  $p_2, p_3$  are related to the adsorption equilibrium constants and partial pressures of A and B, or CO and O<sub>2</sub>.<sup>41,64</sup> Here,  $n$  refers to the dependence on complete shells of nanoclusters. We find that  $\alpha$  affects the full width half-maximum, fwhm,  $p_1$  affects the peak intensity, and  $p_2, p_3$  affect the center of the peak position. From the experimental data,<sup>11</sup> we have that the total pressure is 40 Torr, with a 1:5 molar ratio of CO:O<sub>2</sub>. It is apparent that  $K_{CO} P_{CO}$  and  $K_{O_2} P_{O_2}$  are both dimensionless. Using atm instead of Torr for units of pressures, it holds that  $P_{CO} \approx 0.01$  atm and  $P_{O_2} \approx 0.04$  atm. We allow some variation for the shape of the polyhedra and differing  $K$  values.

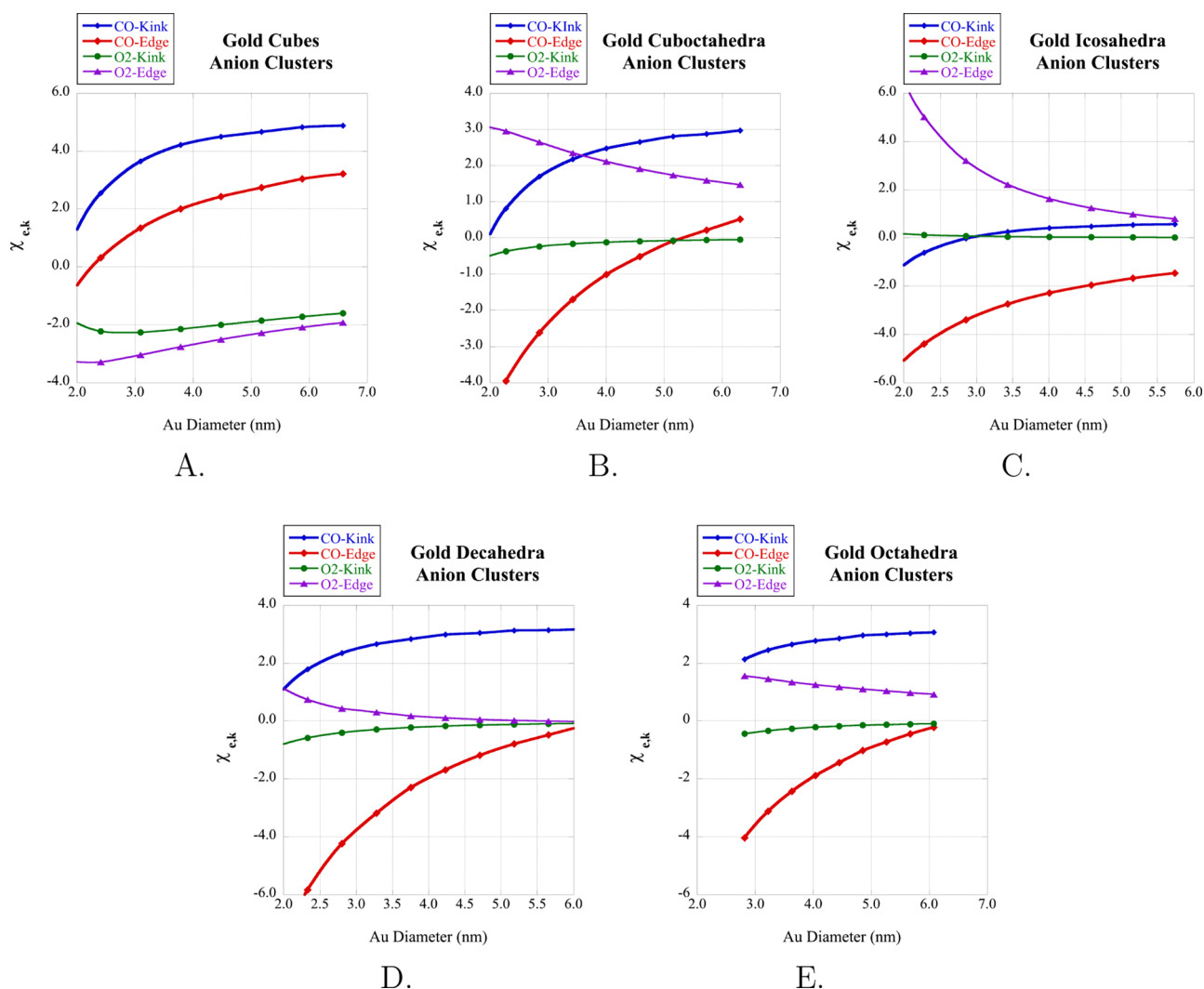
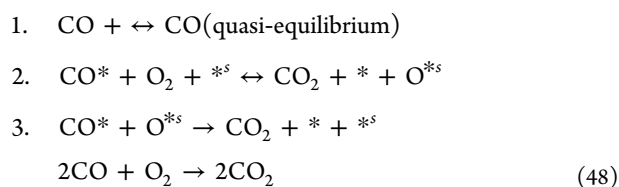


**Figure 2.**  $\chi_k$  and  $\chi_e$  versus  $D$  for adsorption for the five structures considered A. Au-CO and O<sub>2</sub> on truncated cubes. B. Au-CO and O<sub>2</sub> on cuboctahedra. C. Au-CO and O<sub>2</sub> on icosahedra. D. Au-CO and O<sub>2</sub> on decahedra E. Au-CO and O<sub>2</sub> on octahedra. In this and subsequent figures, the data are calculated points related to  $n$  complete shells of nanoclusters.

The L-H mechanism (eq 37) assumes that oxygen is adsorbed on gold with dissociation, which contradicts several studies in the literature suggesting that oxygen atoms are adsorbed at the interface between the metal and the support while not competing with CO for the active sites on the surface of gold clusters. To compare the cluster shape effect in the case of different mechanisms, a mechanism different from L-H in terms of oxygen involvement was thus considered.



From the quasi-equilibria:

$$K_1 = \frac{\theta_{\text{CO}}}{P_{\text{CO}} \cdot \theta_v} \text{ or } \theta_{\text{CO}} = K_1 P_{\text{CO}} \theta_v \quad (49)$$

In mechanism (eq 48), the first step corresponds to molecular adsorption of CO on the metal sites, while the second one addresses the reaction of adsorbed CO with oxygen leading to

the product and an oxygen atom located at the metal–support interface. In the subsequent step, this oxygen atom reacts with adsorbed CO releasing the product and recovering the active sites both on the metal surface ( $*$ ) and at the interface ( $^{*s}$ ). The steady-state approximation for the steps 2 and 3 gives

$$k_2 \theta_{\text{CO}} P_{\text{O}_2} \theta_v^{*s} = k_3 \theta_{\text{CO}} \theta_{\text{O}}^{*s} \quad (50)$$

Thus, we have

$$\theta_{\text{O}}^{*s} = \frac{k_2 P_{\text{O}_2} \theta_v^{*s}}{k_3} \quad (51)$$

The reaction rate is then

$$v = \frac{k_2 K_1 P_{\text{CO}} P_{\text{O}_2}}{(1 + K_1 P_{\text{CO}}) \left(1 + \frac{k_2 P_{\text{O}_2}}{k_3}\right)} \quad (52)$$

The Gibbs energy balance is

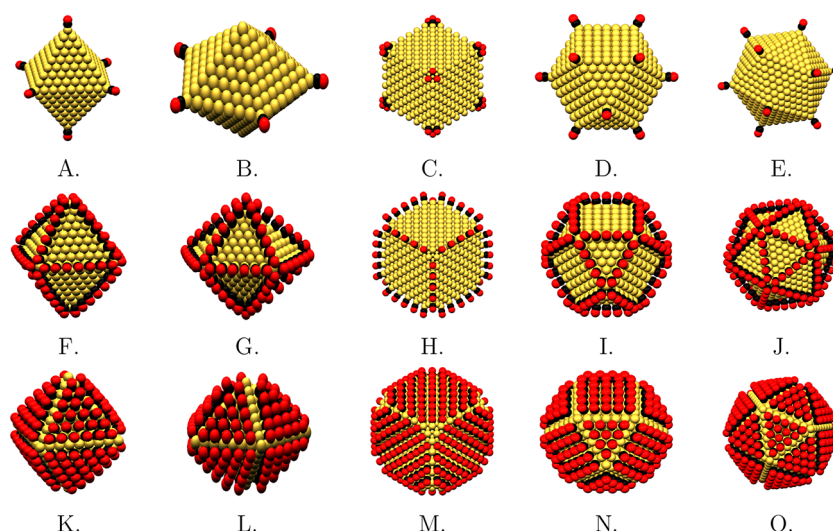


**Figure 3.** Nanoclusters with adsorbed CO on kink, edge, and facet sites. Here the color gold represents a gold atom, black represents carbon, and red oxygen.

$$\begin{aligned}
 2 \quad \Delta G_1 &= \Delta G_{CO^*} - \Delta G_{CO} \\
 1 \quad \Delta G_2 &= \Delta G_{CO_2} + \Delta G_{O^*} - \Delta G_{CO^*} \\
 1 \quad \Delta G_3 &= \Delta G_{CO_2} - \Delta G_{CO^*} - \Delta G_{O^*}.
 \end{aligned} \quad (53)$$

The equilibrium constant of the adsorption step is

$$K_1 = \exp(-\Delta G_1/RT) = \exp(-(\Delta G_{CO^*} - \Delta G_{CO})/RT) \quad (54)$$

We then have

$$\begin{aligned}
 K_1(D) &= K_1^0 \cdot \exp[-(f_{n,e} \cdot \chi_e^{CO}(D) + f_{n,k} \cdot \chi_k^{CO}(D))] \\
 &= K_1^0 \cdot \exp[-\xi_{e,k}^{CO}(D)]
 \end{aligned} \quad (55)$$

where  $\chi_e^{CO}$  is the Gibbs energy of CO adsorption on edges divided by  $RT$ . The rate constant of the second step can be separated into the cluster-size-independent part corresponding to adsorption of oxygen on the support and the cluster-size-dependent part reflecting adsorption of CO on gold:

$$k_2 = g_2 \cdot \exp(-\alpha_2 \Delta G_2/RT) = k_2^0 \cdot \exp[\alpha_2 \cdot \xi_{e,k}^{CO}(D)] \quad (56)$$

A similar expression follows for the size/shape-dependent rate constant of the third step, considering only the nanocluster size dependence for CO adsorption on gold

$$\begin{aligned}
 k_3 &= g_3 \exp(-\alpha_3 \Delta G_3/RT) \\
 &= k_3^0 \exp(\alpha_3 (f_e \chi_e^{CO}(D) + f_k \chi_k^{CO}(D))) \\
 &= k_3^0 \exp(\alpha_3 \xi_{e,k}^{CO}(D))
 \end{aligned} \quad (57)$$

Introducing the size dependence in the rate expression one gets

$$v(D) = \frac{k_2^0 \exp(\alpha_2 (\xi_{e,k}^{CO}(D))) K_1^0 \exp(-(\xi_{e,k}^{CO}(D))) P_{CO} P_{O_2}}{(1 + K_1^0 P_{CO} \exp(-(\xi_{e,k}^{CO}(D)))) (1 + \frac{k_3^0 P_{O_2} \exp(\alpha_3 (\xi_{e,k}^{CO}(D)))}{k_3^0 \exp(\alpha_3 (\xi_{e,k}^{CO}(D)))}}) \quad (58)$$

This results in

$$v(D) = \frac{k_2^0 K_1^0 P_{CO} P_{O_2} \exp((\alpha_2 - 1)(\xi_{e,k}^{CO}(D)))}{(1 + K_1^0 P_{CO} \exp(-(\xi_{e,k}^{CO}(D)))) (1 + \frac{k_3^0 P_{O_2}}{k_3^0} \cdot \exp((\alpha_2 - \alpha_3)(\xi_{e,k}^{CO}(D))))} \quad (59)$$

After simplification, we arrive at:

$$v(D) = \frac{q_1 q_2 \exp[(\alpha_2 - 1)(\xi_{e,k}^{CO}(D))]}{[1 + q_1 \exp(-\xi_{e,k}^{CO}(D))] \left[ 1 + \frac{q_2}{q_3} \exp(\alpha_2 - \alpha_3)(\xi_{e,k}^{CO}(D)) \right]} \quad (60)$$

where  $q_1 = K_1^0 P_{CO}$ ,  $q_2 = k_2^0 P_{O_2}$ , and  $q_3 = k_3^0$ . It is evident that  $q_1$  is dimensionless, and  $q_2, q_3$  have units of  $s^{-1}$ . Also, when the Polanyi parameters of steps 2 and 3 are equal to each other, eq 60 is reduced to the reaction rate expression corresponding to the Eley–Rideal (E-R) mechanism. Similar to the L-H mechanism, we find that  $q_1$  shifts the peak position, while adjusting  $q_2$  affects the peak intensity. We comment that without loss of generality, technically eqs 46, 60 are expressed for one mole of oxygen. To compare with the TOF of CO, one should have  $v(CO) = v(D)/2$ , but this only changes the value of  $p_1$  and  $q_2$ .

## RESULTS AND DISCUSSION

**Au-CO Oxidation.** We use nanoclusters based on shells of atoms, which is possibly an ideal case, given that disorder may occur in clusters. It is known that gold clusters under CO adsorption are dynamic.<sup>68</sup> In other words, exposure to CO causes gold nanoclusters to change morphologically, although annealing may help recover the structure. Likewise, exposure to  $O_2$  can change the morphology of gold clusters.<sup>69</sup> Recent scanning transmission electron microscopy (STEM) experiments may provide a methodology for observing these dynamic features.<sup>70</sup> Defects and morphological changes to clusters can modify the coordination and dynamics of adsorption, but as a first case approach, we use complete shells of atoms to determine the size and shape dependence of the TOF. Further studies may determine the role of defects and morphological changes to the TOF.

The data is shown in Figure 2, where the  $\chi$  values for the five shapes considered are displayed. While clusters with 20 atoms have been fabricated as tetrahedra,<sup>71</sup> it is still challenging to synthesize faceted gold clusters in the size range  $2 \text{ nm} < D < 10 \text{ nm}$ . Icosahedra and cubes were chosen here as examples of clusters with (111) and (100) surfaces, while cuboctahedra have both and are used extensively for DFT modeling. Experiments reveal that the top site on gold surfaces is preferred for CO adsorption.<sup>72</sup> Many studies of Au-CO catalysis of nanogold on

oxide substrates indicate that low coordinated sites also drive the reaction.<sup>40,73–75</sup> In the case of the truncated cube, edge sites have  $cn = 5$ , (see Table 1), while kink sites have  $cn = 7$ . Normally, the fcc cube has 3-fold coordinated corner atoms.<sup>12</sup> When these are removed, the “subsurface” atoms underneath in the truncated cube are 7-fold coordinated, while in both cases the edge atoms are 5-fold coordinated.<sup>13</sup> The calculated  $\Delta G$  values were used to determine all the  $\chi_e$  and  $\chi_k$  needed for the turnover frequency computation. These Gibbs adsorption energies were determined from MATLAB code using eq 23 above. As is mentioned in eqs 46 and (60) above, the  $\chi_{e,k}$  values are important for the calculation of the TOF as defined previously. We mention here that in our model, adsorbed species are separated by edge, kink, or facet sites, and are randomly added until maximum coverage. In this model, these adsorption sites have different Gibbs adsorption energies, but they are not mixed to simplify the calculations. Also, it is assumed that local distortions due to adsorption, do not affect the bonding energy; thus, the catalysis proceeds on the polyhedral surfaces. In Figure 3, models of adsorbed CO on gold clusters for the five shapes are given. For O<sub>2</sub>, the adsorption energy is negative when the generalized coordination number  $\overline{CN}_i < 6$ . In Figure 4, models of O<sub>2</sub> adsorbed on facet and edge sites of polyhedra are shown.

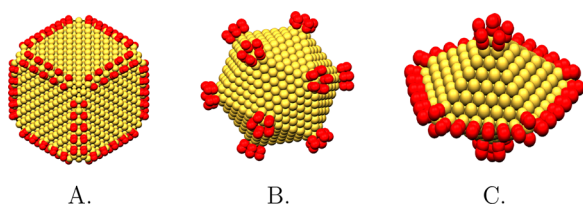


**Figure 4.** O<sub>2</sub> facet sites on truncated cubes and on edge sites of icosahedra and decahedra. In this model, all atoms are on the on-top sites to simplify the calculations. Reference 76 also has O<sub>2</sub> adsorbed on the on-top sites for gold subnanoclusters.

In agreement with previous work,<sup>64</sup> we find both the L-H and E-R mechanisms have peak positions which vary with the different polyhedra. In Figure 5A, the TOF was computationally modeled using the calculated Gibbs adsorption energy and eq 46. The experimental data from,<sup>11</sup> exhibit rather wide error bars in the measured diameters of the gold clusters. The line fit to the experimental TOF is a line best fit by eye.<sup>11</sup> The TOF plots for the five shapes studied, in Figure 5, were made under the approximation that only one shape at a time is observed for the experimental conditions. Also, we note that the experimental data that generated the TOF had spherical nanoparticles instead of faceted polyhedra.<sup>8,11</sup> In Figure 5B, we show the results for the E-R mechanism and eq 60. Table 5 tabulates the shape

**Table 5. Shape Parameters for the Au-CO Oxidation TOF via the L-H Mechanism ( $p_i$ ) and the E-R Mechanism ( $q_i$ ) (Modeling Parameters for Figure 5A,B)<sup>a</sup>**

structure	$p_1$ ( $s^{-1}$ )	$p_2$	$p_3$	$q_1$	$q_2$ ( $s^{-1}$ )	$q_3$ ( $s^{-1}$ )
cuboctahedra	13	1.0	10	0.35	1.0	10.0
cube	17	10	0.7	0.30	3.0	10.0
icosahedron	25	1.1	17	0.20	1.3	10.0
octahedron	34	0.8	17	0.15	1.5	10.0
decahedron	95	0.8	30	0.10	2.0	10.0

<sup>a</sup>This data assumes only one shape is present in the sample for any given experiment. Here  $p_2$ ,  $p_3$ , and  $q_1$  are dimensionless.

parameters used to model the TOF for the L-H and E-R mechanisms. While the better fits to the data are from the octahedra and decahedra (perhaps due to more data points), it remains that a possibly fair criticism of the model is that the  $\chi$  values may not be large enough to account for the sharp experimental peak in the TOF.

A typical value for the Polanyi parameter (i.e.,  $\alpha = 0.5$ ), was chosen similar to reference 64 for both the L-H and E-R mechanisms. No experimental TOF has been also ascertained for a distribution involving only one type of polyhedra. In Figure 5, the fits to the TOF curves with either a Gaussian curve or a

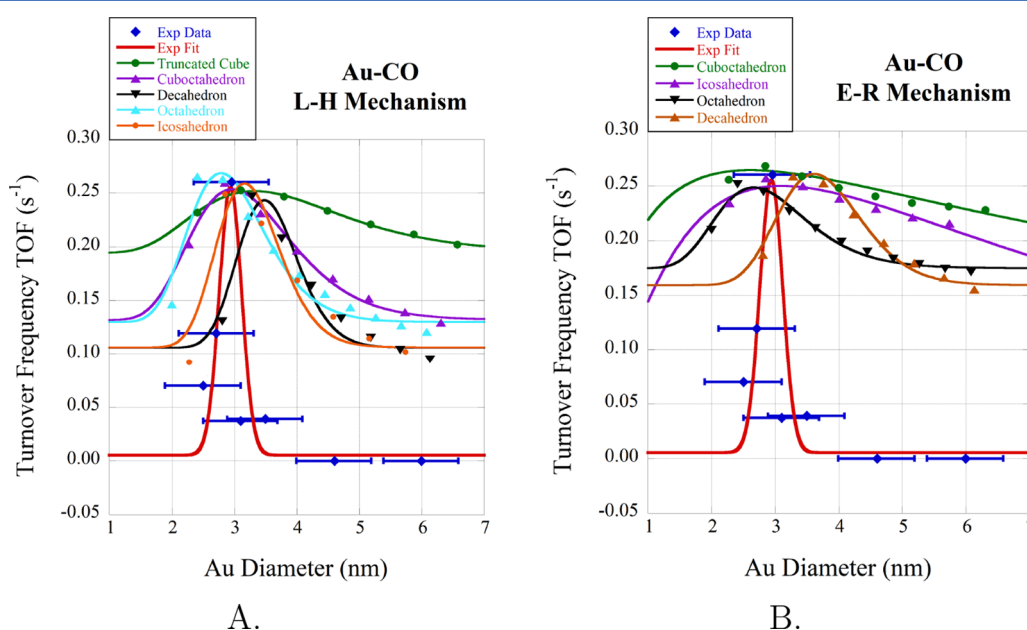


**Figure 5.** A. TOF data fit to eq 46, for separate distributions of shapes with anion gold clusters. Experimental data from ref 11. B. TOF data fit to eq 60 and the E-R mechanism.

log-normal are given. The icosahedron, truncated cube, octahedron, decahedron, and the cuboctahedron are asymmetric and better fit to a log-normal ( $R^2 > 0.91$ ), while the experimental data are better fit to a Gaussian. The log-normal has a mean and variance given by

$$\bar{\mu} = \exp\left(\mu + \frac{\sigma^2}{2}\right) \quad (61)$$

$$\bar{\sigma}^2 = [\exp(\sigma^2) - 1]\exp(2\mu + \sigma^2) \quad (62)$$

where  $\mu$  and  $\sigma$  are related to the log-normal distribution. Table 6 displays the Gaussian and log-normal fits to the above equations.

**Table 6. Mean and Standard Deviation for the Au-CO Oxidation TOF via the L-H Mechanism (Modeling Parameters for Figure 5A), with Gold Anion Clusters<sup>a</sup>**

structure	$\bar{\mu}$ LH	$\bar{\sigma}$ LH	$\bar{\mu}$ ER	$\bar{\sigma}$ ER
exp fit	2.937	0.181	2.937	0.181
octahedron	2.998	0.666	2.959	0.881
decahedron	3.584	0.496	3.793	0.739
icosahedron	3.286	0.527	12.329	15.148
cuboctahedron	3.317	0.918	20.922	36.282
truncated cube	3.999	1.456	NA	NA

<sup>a</sup>The last two columns refer to the E-R mechanism of the clusters, Figure 5B.

The TOF is modeled with anionic gold clusters, with anions mimicking the effect of a gold cluster on an oxide substrate. Although the experimental TOF has a narrow fwhm, the error bars in the size estimation are wide and within the simulated data. Our simulations suggest that coordination and values for  $\chi$  or  $\Delta G$  are important factors in determining the experimental data. Although free-standing anionic nanoclusters were modeled here, similar results might be expected for deposited half-clusters on a substrate.

The mass activity is basically the product of the dispersion and the TOF<sup>77</sup>

$$MA_{Au} = \frac{\mathcal{F}}{AW_{Au}} \frac{N_S}{N_T} \frac{v(D)}{10^3} (\text{A/mg}_{Au}) \quad (63)$$

where  $\mathcal{F}$  is the Faraday constant, 96,485 C/mol, and  $AW_{Au}$  is the atomic weight of gold, 196.967 g/mol. In principle, this gives an exact form of the mass activity. The clusters with a narrow TOF, or icosahedra, have a good correlation with mass activity from the experimental data of the CO oxidation reaction. Note that the experimental data (Figure 6) are in arbitrary units, which were reduced by 20 for comparison with eq 63.<sup>11</sup> Although we model the MA based on the TOF of individual polyhedra, we note that an alternative method based on specific activity and surface area has been used for the oxygen reduction of platinum nanopolyhedra.<sup>78</sup> We acknowledge that a more detailed understanding of the kinetic parameters  $K$ , used for the TOF may result in maxima of the MA differing for the specific polyhedra studied. The data for the polyhedra not shown did not result in a peak in the mass activity. Table 7 shows the log-normal fitting to the mass activity for specific polyhedra.

**Table 7. Mean and Standard Deviation for the Mass Activity via the L-H Mechanism (Modeling Parameters for Figure 6A), with Gold Anion Clusters<sup>a</sup>**

structure	$\bar{\mu}$ LH	$\bar{\sigma}$ LH	$\bar{\mu}$ ER	$\bar{\sigma}$ ER
exp fit	3.205	0.738	3.205	0.738
octahedron	2.879	0.740	2.857	1.270
decahedron	3.521	0.559	3.695	0.766
icosahedron	3.055	0.585	NA	NA

<sup>a</sup>The last two columns refer to the mass activity for the E-R mechanism for the clusters, Figure 6B.

To account for several shapes with independent distributions, one can sum over the morphology:<sup>79</sup>

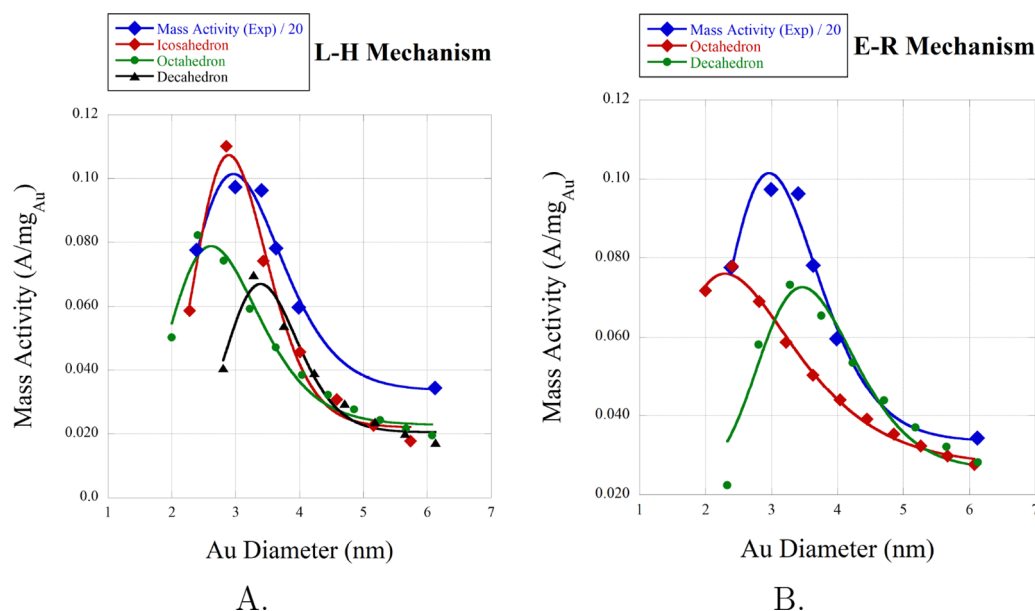


**Figure 6.** A. Mass activity data fit to eq 63, for separate distributions of shapes with anion gold clusters and the L-H mechanism. Experimental data from.<sup>11</sup> B. Mass activity data fit to eq 63 and the E-R mechanism.

$$v(D) = \sum_i \rho_i \cdot v_i(D) \quad (64)$$

where  $i$  is one of many possible shapes, perhaps those studied herein. This may provide a method of approach for gold nanoclusters with several types of polyhedra. Such an approach is suggested for future consideration.

Given the importance of edge and kink sites relative to facet ones with regard to catalytic activity, the surface dispersion was determined for the five clusters under study. This may provide insight into the reasons for the individual polyhedral activity when compared among the five clusters. In Figure 7, the surface

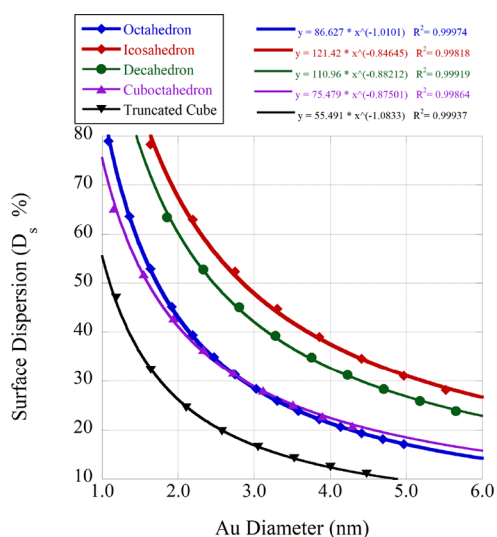


**Figure 7.** Surface dispersion for the five gold shapes under consideration.

dispersion  $D_s = (N_e + N_k)/N_s \cdot 100\%$  is plotted vs the gold diameter for the five shapes from the equations in Table 1. It is clear that  $D_s$  is related to the fraction of more active edge and kink sites to the total number of surface sites. As can be seen from the data, the surface dispersion is greatest for the icosahedron, with the cuboctahedron and truncated cubes exhibiting smaller dispersion.

## CONCLUSION

These results lend insight into a long unsolved problem, namely, an explanation of the experimental data for the TOF and mass activity of the oxidation of carbon monoxide on gold nanoclusters. Although the experimental fit to the TOF data is only a line estimate, the current analysis has a wider full width at half-maximum, (fwhm) than that of the experiment. These results confirm that coordination, shape, and  $\Delta G$  have a dramatic influence on the catalysis of reactions. We provide explicit relationships between coordination and shape. Calculations of  $\Delta G$  also show that low coordination leads to higher values, and this in turn affects the TOF. Modeling with anionic clusters shows that the fwhm decreases for clusters on oxide substrates. The data is made quantitative through modeling with either a log-normal or Gaussian distribution. Overall, good fit to the data was given by icosahedra for the L-H mechanism for both the TOF and mass activity. In general, the E-R mechanism resulted in flatter curves when fit to the TOF, although a better match was obtained for octahedra and decahedra. While both mechanisms resulted in peaked data, it remains that neither

method reproduces the experimental data exactly. The authors hope that these results encourage further experimental work and theoretical modeling.

## AUTHOR INFORMATION

### Corresponding Author

Forrest H. Kaatz – *Institutional Research, Mesalands Community College, Tucumcari, New Mexico 88401, United States*; [orcid.org/0000-0001-7912-0627](https://orcid.org/0000-0001-7912-0627); Email: [fhkaatz@gmail.com](mailto:fhkaatz@gmail.com)

### Authors

Dmitry Yu. Murzin – *Industrial Chemistry and Reaction Engineering, Abo Akademi University, Turku 20500, Finland*; [orcid.org/0000-0003-0788-2643](https://orcid.org/0000-0003-0788-2643)

Adhemar Bultheel – *Department Computer Sci., KU Leuven, 3001 Heverlee, Belgium*; [orcid.org/0000-0001-9562-5297](https://orcid.org/0000-0001-9562-5297)

Complete contact information is available at: <https://pubs.acs.org/10.1021/acscatal.1c00892>

### Author Contributions

F.H.K. conceived of the project, did the data analysis, and wrote the initial draft. D.Y.M. analyzed the kinetic mechanisms and derived the rate equations. A.B. wrote the MATLAB code (Note: All computational modeling uses original code developed by the authors compatible with MATLAB 2021a). All authors contributed to the final version and approved the article as submitted.

### Funding

This research did not receive any specific grant from funding agencies in the public, commercial, or not-for-profit sectors.

### Notes

The authors declare no competing financial interest.

## REFERENCES

- Boudart, M. Catalysis by supported metals. *Adv. Catal.* **1969**, *20*, 153–166.
- Falicov, L. M.; Somorjai, G. A. Correlation between catalytic activity and bonding and coordination number of atoms and molecules on transition metal surfaces: Theory and experimental evidence. *Proc. Natl. Acad. Sci. U. S. A.* **1985**, *82*, 2207–2211.
- Shi, Y.; Lyu, Z.; Zhao, M.; Chen, R.; Nguyen, Q. N.; Xia, Y. Noble-metal nanocrystals with controlled shapes for catalytic and electrocatalytic applications. *Chem. Rev.* **2021**, *121* (2), 649–735.
- Lambie, S. G.; Weal, G. R.; Blackmore, C. E.; Palmer, R. E.; Garden, A. L. Contrasting motif preferences of platinum and gold nanoclusters between 55 and 309 atoms. *Nanoscale Adv.* **2019**, *1*, 2416.
- Ishida, T.; Murayama, T.; Taketoshi, A.; Haruta, M. Importance of size and contact structure of gold nanoparticles for the genesis of unique catalytic processes. *Chem. Rev.* **2020**, *120*, 464–525.
- Haruta, M.; Kobayashi, T.; Sano, H.; Yamada, N. Novel gold catalysts for the oxidation of carbon monoxide at a temperature far below 0°C. *Chem. Lett.* **1987**, *16* (2), 405–408.
- Haruta, M.; Yamada, N.; Koybayashi, T.; Iijima, S. Gold catalysts prepared by coprecipitation for low-temperature oxidation of hydrogen and of carbon monoxide. *J. Catal.* **1989**, *115* (2), 301–309.
- Haruta, M. Size- and support-dependency in the catalysis of gold. *Catal. Today* **1997**, *36* (1), 153–166.
- Hutchings, G. J.; Brust, M.; Schmidbaur, H. Gold - an introductory perspective. *Chem. Soc. Rev.* **2008**, *37* (9), 1759–1765.
- Bamwenda, G. R.; Tsubota, S.; Nakamura, T.; Haruta, M. The influence of the preparation methods on the catalytic activity of platinum and gold supported on TiO<sub>2</sub> for CO oxidation. *Catal. Lett.* **1997**, *44*, 83–87.

- (11) Valden, M.; Lai, X.; Goodman, D. W. Onset of catalytic activity of gold clusters on titania with the appearance of nonmetallic properties. *Science* **1998**, *281*, 1647–1650.
- (12) Kaatz, F. H.; Bultheel, A. Magic mathematical relationships for nanoclusters. *Nanoscale Res. Lett.* **2019**, *14* (1), 150.
- (13) Kaatz, F. H.; Bultheel, A. Magic mathematical relationships for nanoclusters - errata and addendum. *Nanoscale Res. Lett.* **2019**, *14* (1), 295.
- (14) Kleis, J.; Greeley, J. P.; Romero, N. A.; Morozov, V. A.; Falsig, H.; Larsen, A. H.; Lu, J.; Mortensen, J. J.; Dulak, M.; Thygesen, K. S.; Nørskov, J. K.; Jacobsen, K. W. Finite size effects in chemical bonding: From small clusters to solids. *Catal. Lett.* **2011**, *141*, 1067–1071.
- (15) Li, L.; Larsen, A. H.; Romero, N. A.; Morozov, V. A.; Glinsvad, C.; Abild-Pedersen, F.; Greeley, J.; Jacobsen, K. W.; Nørskov, J. K. Investigation of catalytic finite-size-effects of platinum clusters. *J. Phys. Chem. Lett.* **2013**, *4*, 222–226.
- (16) Hoover, W. G.; Hindmarsh, A. C.; Holian, B. L. Number dependence of small-crystal thermodynamic properties I. *J. Chem. Phys.* **1972**, *57* (5), 1980–1985.
- (17) Wautelet, M.; Shirinyan, A. S. Thermodynamics: nano vs. macro. *Pure Appl. Chem.* **2009**, *81* (10), 1921–1930.
- (18) Fichthorn, K. A.; Yan, T. Shapes and shape transformations of solution-phase metal particles in the sub-nanometer to nanometer size range: Progress and challenges. *J. Phys. Chem. C* **2021**, *125*, 3668–3679.
- (19) Hill, T. L. A different approach to nanothermodynamics. *Nano Lett.* **2001**, *1* (5), 273–275.
- (20) Bedeaux, D.; Kjelstrup, S. Hill's nano-thermodynamics is equivalent with Gibbs' thermodynamics for surfaces of constant curvatures. *Chem. Phys. Lett.* **2018**, *707*, 40–43.
- (21) Fu, Q.; Xue, Y. Q.; Cui, Z. Size- and shape-dependent surface thermodynamic properties of nanocrystals. *J. Phys. Chem. Solids* **2018**, *116*, 79–85.
- (22) Bond, G. C. The effect of the metal to non-metal transition on the activity of gold catalysts. *Faraday Discuss.* **2011**, *152*, 277–291.
- (23) Zhdanov, V. P. Kinetic models of CO oxidation on gold nanoparticles. *Surf. Sci.* **2014**, *630*, 286–293.
- (24) Calle-Vallejo, F.; Martinez, J. I.; Garcia-Lastra, J. M.; Sautet, P.; Loffreda, D. Fast prediction of adsorption properties for platinum nanocatalysts with generalized coordination numbers. *Angew. Chem., Int. Ed.* **2014**, *53*, 8316–8319.
- (25) Calle-Vallejo, F.; Tymoczko, J.; Colic, V.; Vu, Q.-H.; Pohl, M. D.; Morgenstern, K.; Loffreda, D.; Sautet, Ph.; Schuhmann, W.; Bandarenka, A. S. Finding optimal surface sites on heterogeneous catalysts by counting nearest neighbors. *Science* **2015**, *350* (6257), 185–189.
- (26) Ma, X.; Xin, H. Orbitalwise coordination number for predicting adsorption properties of metal nanocatalysts. *Phys. Rev. Lett.* **2017**, *118*, 036101.
- (27) Xu, H.; Cheng, D.; Gao, Y.; Zeng, X. C. Assessment of catalytic activities of gold nanoclusters with simple structure descriptors. *ACS Catal.* **2018**, *8*, 9702–9710.
- (28) Lin, X.; Yang, B.; Benia, H.; Myrach, Ph.; Yulikov, M.; Aumer, A.; Brown, M. A.; Sterrer, M.; Bondarchuk, O.; Kieseritzky, E.; Rocker, J.; Risse, T.; Gao, H.-J.; Nilius, N.; Freund, H.-J. Charge-mediated adsorption behavior of CO on MgO-supported Au clusters. *J. Am. Chem. Soc.* **2010**, *132*, 7745–7749.
- (29) Wang, Y. G.; Yoon, Y.; Glezakou, V. A.; Li, J.; Rousseau, R. The role of reducible oxide-metal cluster charge transfer in catalytic processes: New insights on the catalytic mechanism of CO oxidation on Au/TiO<sub>2</sub> from ab initio molecular dynamics. *J. Am. Chem. Soc.* **2013**, *135*, 10673–10683.
- (30) Joshi, A. M.; Tucker, M. H.; Delgass, W. N.; Thomson, K. T. CO adsorption on pure and binary-alloy gold clusters: A quantum chemical study. *J. Chem. Phys.* **2006**, *125*, 194707.
- (31) Fernandez, E. M.; Balbas, L. C. Multiple adsorption of molecular oxygen on small Au/Pd cationic clusters at finite temperature. A van der Waals density functional study. *J. Chem. Phys.* **2016**, *144*, 224308.
- (32) Peng, H.; Qi, W. H.; Li, S.; Ji, W. Modeling the phase stability of Janus, core-shell, and alloyed Ag-Cu and Ag-Au nanoparticles. *J. Phys. Chem. C* **2015**, *119*, 2186–2195.
- (33) Reuter, K.; Scheffler, M. Composition, structure and stability of RuO<sub>2</sub> as a function of oxygen pressure. *Phys. Rev. B: Condens. Matter Mater. Phys.* **2001**, *65*, 035406.
- (34) Gross, A. *Theory of Solid/Electrolyte Interfaces*, Vol 7; Wiley-VCH verlag GmbH, 2020.
- (35) Granda-Marulanda, L. P.; Rendón-Calle, A.; Builes, S.; Illas, F.; Koper, M. T. M.; Calle-Vallejo, F. A semiempirical method to detect and correct DFT-based gas-phase errors and its application in electrocatalysis. *ACS Catal.* **2020**, *10*, 6900–6907.
- (36) Christensen, R.; Hansen, H. A.; Vegge, T. Identifying systematic DFT errors in catalytic reactions. *Catal. Sci. Technol.* **2015**, *5*, 4946–4949.
- (37) Davis, J. B. A.; Baletto, F.; Johnston, R. L. The effect of dispersion correction on the adsorption of CO on metallic nanoparticles. *J. Phys. Chem. A* **2015**, *119*, 9703–9709.
- (38) Jorgensen, M.; Gronbeck, H. Scaling relations and kinetic Monte Carlo simulations to bridge the materials gap in heterogeneous catalysis. *ACS Catal.* **2017**, *7*, 5054–5061.
- (39) Falsig, H.; Hvolbæk, B.; Kristensen, I. S.; Jiang, T.; Bligaard, T.; Christensen, C.-H.; Nørskov, J.-K. Trends in the catalytic CO oxidation activity of nanoparticles. *Angew. Chem., Int. Ed.* **2008**, *47*, 4835–4839.
- (40) Jiang, T.; Mowbray, D. J.; Dobrin, S.; Falsig, H.; Hvolbæk, B.; Bligaard, T.; Nørskov, J. K. Trends in CO oxidation rates for metal nanoparticles and close-packed, stepped, and kinked surfaces. *J. Phys. Chem. C* **2009**, *113* (24), 10548–10553.
- (41) Murzin, D. Y. Kinetic analysis of cluster size dependent activity and selectivity. *J. Catal.* **2010**, *276*, 85–91.
- (42) Li, Y.; Lin, H.; Zhou, W.; Sun, L.; Samanta, D.; Mirkin, C. A. Corner-, edge-, and facet-controlled growth of nanocrystals. *Science Adv.* **2021**, *7*, No. eabf1410.
- (43) Bligaard, T.; Nørskov, J. K.; Dahl, S.; Matthiesen, J.; Christensen, C. H.; Sehested, J. The Brønsted–Evans–Polanyi relation and the volcano curve in heterogeneous catalysis. *J. Catal.* **2004**, *224*, 206–217.
- (44) Brønsted, J. N. Acid and basic catalysis. *Chem. Rev.* **1928**, *5* (3), 231–338.
- (45) Pallassana, V.; Neurock, M. Electronic factors governing ethylene hydrogenation and dehydrogenation activity of pseudomorphic Pd<sub>ML</sub>/Re(0001), Pd<sub>ML</sub>/Ru(0001), Pd(111), and Pd<sub>ML</sub>/Au(111) surfaces. *J. Catal.* **2000**, *191* (2), 301–317.
- (46) Nørskov, J. K.; Bligaard, T.; Logadottir, A.; Bahn, S.; Hansen, L. B.; Bollinger, M.; Benggaard, H.; Hammer, B.; Sljivancanin, Z.; Mavrikakis, M.; Xu, Y.; Dahl, S.; Jacobsen, C. J. H. Universality in heterogeneous catalysis. *J. Catal.* **2002**, *209*, 275–278.
- (47) Panov, G.; Parfenov, M. G.; Parmon, V. N. The Brønsted-Evans-Polyani correlations in oxidation catalysis. *Catal. Rev.: Sci. Eng.* **2015**, *57* (4), 436–477.
- (48) Kropp, T.; Mavrikakis, M. Brønsted-Evans-Polyani relation for CO oxidation on metal oxides following the Mars–van Krevelen mechanisms. *J. Catal.* **2019**, *377*, 577–581.
- (49) Ding, Z. B.; Maestri, M. Development and assessment of a criterion for the application of Brønsted-Evans-Polyani relations for dissociation catalytic reactions at surfaces. *Ind. Eng. Chem. Res.* **2019**, *58*, 9864–9874.
- (50) Liu, J. X.; Pilot, I. A. W.; Su, Y.; Zijlstra, B.; Hensen, E. J. M. Optimum particle size for gold-catalyzed CO oxidation. *J. Phys. Chem. C* **2018**, *122* (15), 8327–8340.
- (51) Behraves, E.; Melander, M. M.; Warna, J.; Salmi, T.; Honkala, K.; Murzin, D. Y. Oxidative dehydrogenation of ethanol on gold: Combination of kinetic experiments and computation approach to unravel the reaction mechanism. *J. Catal.* **2021**, *394*, 193–205.
- (52) Moruzzi, V. L.; Janak, J. F.; Schwarz, K. Calculated thermal properties of metals. *Phys. Rev. B: Condens. Matter Mater. Phys.* **1988**, *37* (2), 790–799.
- (53) Ostanin, S. A.; Trubitsin, V. Y. A simple model for calculating the P-T phase diagram of Ti. *J. Phys.: Condens. Matter* **1997**, *9*, L491–L496.

- (54) Xiong, S. Y.; Qi, W. H.; Huang, B.; Wang, M. P.; Li, Y. J. Size and shape dependent Gibbs free energy and phase stability of Titanium and Zirconium nanoparticles. *Mater. Chem. Phys.* **2010**, *120*, 446–451.
- (55) Chen, Q.; Sundman, B. Calculation of Debye temperature for crystalline structures—a case study on Ti, Zr, and Hf. *Acta Mater.* **2001**, *49*, 947–961.
- (56) Sun, C. Q. Size dependence of nanostructures: Impact of bond order deficiency. *Prog. Solid State Chem.* **2007**, *35* (1), 1–159.
- (57) Maioli, P.; Stöll, T.; Saucedo, H. E.; Valencia, I.; Demessence, A.; Bertorelle, F.; Crut, A.; Vallée, F.; Garzón, I. L.; Cerullo, G.; Del Fatti, N. Mechanical vibrations of atomically defined metal clusters: From nano- to molecular-size oscillators. *Nano Lett.* **2018**, *18*, 6842–6849.
- (58) Qi, W. H.; Wang, M. P.; Liu, Q. H. Shape factor of nonspherical nanoparticles. *J. Mater. Sci.* **2005**, *40*, 2737–2739.
- (59) Jiang, Q.; Liang, L. H.; Zhao, D. S. Lattice contraction and surface stress of fcc nanocrystals. *J. Phys. Chem. B* **2001**, *105* (27), 6275–6277.
- (60) NIST - JANAF thermochemical tables, <https://janaf.nist.gov/>.
- (61) Li, H.; Li, L.; Pedersen, A.; Gao, Y.; Khetrpal, N.; Jonsson, H.; Zeng, X. C. Magic-number gold nanoclusters with diameters from 1 to 3.5 nm: Relative stability and catalytic activity for CO oxidation. *Nano Lett.* **2015**, *15* (1), 682–688.
- (62) Rossi, K.; Asara, G. G.; Baletto, F. A genomic characterization of monometallic particles. *Phys. Chem. Chem. Phys.* **2019**, *21*, 4888–4898.
- (63) Strizhak, P. E. Nanosize effects in heterogeneous catalysis. *Theor. Exp. Chem.* **2013**, *49* (1), 2–21.
- (64) Murzin, D. Y. Cluster size dependent kinetics: Analysis of different reaction mechanisms. *Catal. Lett.* **2015**, *145*, 1948–1954.
- (65) Murzin, D. Y. Size-dependent heterogeneous catalytic kinetics. *J. Mol. Catal. A: Chem.* **2010**, *315*, 226–230.
- (66) Zhdanov, V. P.; Kasemo, B. Simulations of the reaction kinetics on nanometer supported catalyst particles. *Surf. Sci. Rep.* **2000**, *39*, 25–104.
- (67) Chen, H. T.; Chang, J. G.; Ju, S. P.; Chen, H. L. First-principle calculations on CO oxidation catalyzed by a gold nanoparticle. *J. Comput. Chem.* **2009**, *31* (2), 258–265.
- (68) Hrbek, J.; Hoffmann, F. M.; Park, J. B.; Liu, P.; Stacchiola, D.; Hoo, Y. S.; Ma, S.; Nambu, A.; Rodriguez, J. A.; White, M. G. Adsorbate-driven morphological changes of a gold surface at low temperatures. *J. Am. Chem. Soc.* **2008**, *130*, 17272–17273.
- (69) Chmielewski, A.; Meng, J.; Zhu, B.; Gao, Y.; Guesmi, H.; Prunier, H.; Alloyeau, D.; Wang, G.; Louis, C.; Delannoy, L.; Afanasiev, P.; Ricolleau, C.; Nelayah, J. Reshaping dynamics of gold nanoparticles under H<sub>2</sub> and O<sub>2</sub> at atmospheric pressure. *ACS Nano* **2019**, *13*, 2024–2033.
- (70) De wael, A.; De Backer, A.; Jones, L.; Varambhia, A.; Nellist, P. D.; Van Aert, S. Measuring dynamic structural changes of nanoparticles at the atomic scale using scanning transmission electron microscopy. *Phys. Rev. Lett.* **2020**, *124*, 106105.
- (71) Li, J.; Li, X.; Zhai, H. J.; Wang, L. S. Au<sub>20</sub>: A tetrahedral cluster. *Science* **2003**, *299*, 864–867.
- (72) Yoshida, H.; Kuwauchi, Y.; Jinschek, J. R.; Sun, K.; Tanaka, S.; Kohyama, M.; Shimada, S.; Haruta, M.; Takeda, S. Visualizing gas molecules interacting with supported nanoparticulate catalysts at reaction conditions. *Science* **2012**, *335* (6066), 317–319.
- (73) Lopez, N.; Janssens, T. V. W.; Clausen, B. S.; Xu, Y.; Mavrikakis, M.; Pedersen, T. B.; Nørskov, J. K. On the origin of the catalytic activity of gold nanoparticles for low-temperature CO oxidation. *J. Catal.* **2004**, *223*, 232–235.
- (74) Yim, W. L.; Nowitzki, T.; Necke, M.; Schnars, H.; Nickut, P.; Biener, J.; Biener, M. M.; Zielasek, V.; Al-Shamery, K.; Klüner, T.; Bäumer, M. Universal phenomena of CO adsorption on gold surfaces with low-coordinated sites. *J. Phys. Chem. C* **2007**, *111* (1), 445–451.
- (75) Janssens, T. V. W.; Clausen, B. S.; Hvolbæk, B.; Falsig, H.; Christensen, C. H.; Bligaard, T.; Nørskov, J. K. Insights into the reactivity of supported Au nanoparticles: combining theory and experiments. *Top. Catal.* **2007**, *44* (1–2), 15–26.
- (76) Yadav, J.; Saini, S. Atop adsorption of oxygen on small sized gold clusters: Analysis of size and site reactivity from restructuring perspective. *Comput. Theor. Chem.* **2020**, *1191*, 113014.
- (77) Gasteiger, H. A.; Markovic, N. M. Just a dream - or future reality? *Science* **2009**, *324*, 48–49.
- (78) Rossi, K.; Asara, G. G.; Baletto, F. Structural screening and design of Platinum nanosamples for oxygen reduction. *ACS Catal.* **2020**, *10*, 3911–3920.
- (79) Murzin, D. Y.; Simakova, I. L. Influence of cluster size distribution on cluster size dependent catalytic kinetics. *Catal. Lett.* **2011**, *141*, 982–986.